Microstructure and Fracture Behavior of (Co)Injection-Molded Polyamide 6 Composites with Short Glass/Carbon Fiber Hybrid Reinforcement

S. Solomon,[1] A. Abu Bakar,[1] Z. A. Mohd Ishak,[1] U. S. Ishiaku,[2] H. Hamada[2]

[1]*School of Materials and Mineral Resources Engineering, Engineering Campus, Universiti Sains Malaysia, 14300 Nibong Tebal, Penang, Malaysia.*
[2]*Advanced Fibro-Science, Kyoto Institute of Technology, Matsugasaki, Sakyo-ku, Kyoto 606-8585, Japan*

Received 26 February 2004; accepted 9 December 2004
DOI 10.1002/app.21794
Published online in Wiley InterScience (www.interscience.wiley.com).

ABSTRACT: The mechanical and fracture properties of injection molded short glass fiber)/short carbon fiber reinforced polyamide 6 (PA 6) hybrid composites were studied. The short fiber composites of PA 6 glass fiber, carbon fiber, and the hybrid blend were injection molded using a conventional machine whereas the two types of sandwich skin–core hybrids were coinjection molded. The fiber volume fraction for all formulations was fixed at 0.07. The overall composite density, volume, and weight fraction for each formulation was calculated after composite pyrolysis in a furnace at 600°C under nitrogen atmosphere. The tensile, flexural, and single-edge notch-bending tests were performed on all formulations. Microstructural characterizations involved the determination of thermal properties, skin–core thickness, and fiber length distributions. The carbon fiber/PA 6 (CF/PA 6) formulation exhibits the highest values for most tests. The sandwich skin-core hybrid composites exhibit values lower than the CF/PA 6 and hybrid composite blends for the mechanical and fracture tests. The behaviors of all composite formulations are explained in terms of mechanical and fracture properties and its proportion to the composite strength, fiber orientation, interfacial bonding between fibers and matrix, nucleating ability of carbon fibers, and the effects of the skin and core structures. Failure mechanisms of both the matrix and the composites, assessed by fractographic studies in a scanning electron microscope, are discussed. J Appl Polym Sci 97: 957–967, 2005

Key words: microstructure; polyamide; composites

INTRODUCTION

Polyamide 6 (PA 6) is a semicrystalline material widely used as a matrix in the production of short fiber reinforced thermoplastic (SFRTP) composites. This is because of their desirable properties such as high strength, stiffness, and resistance to nonpolar solvents.[1] However, PA 6 has some other characteristics that limit its use in many applications; for example, it has poor low-temperature toughness and is quite notch-sensitive. The addition of glass fiber reinforcement is known to improve the stiffness, strength, and high temperature performance of polymeric materials whereas the incorporation of carbon fibers leads to enhanced thermal resistance and strength in the material.[2–4]

The mechanical properties of SFRTPs are governed by complex interactions of internal or microstructure-related parameters such as types of matrix, types and volume fraction of fibers, fiber aspect ratio, and fiber orientation distributions, as well as the fiber–matrix interface. This fiber–matrix interface is dependent upon the nature, shape, and surface toughness of the fibers. In addition, there are other external factors that must be considered, namely the rate and mode of testing and also the surrounding environment.

In injection molded short fiber composites, a three-layer (skin–core–skin) structure is usually developed.[8,9] Such structures (where the skin may amount up to 50% of the cross-sectional area) yield very strong composites, which combine high strength with better toughness. There is a good characterization of the skin and core materials with respect to their macroscopic properties.[2,8] However, most of the studies on SFRTPs have focused on materials prepared using conventional injection molding techniques and not using coinjection molding.

The coinjection molding process was first described and developed by ICI in 1970 to overcome surface finish limitations inherent in the structural foam process, which has a rough surface finish.[10,11] However, over the years, the coinjection molding process has been used for a variety of purposes and to curb a variety of problems, the first and foremost reason being to reduce material cost. Carbon fibers are very expensive compared to glass fibers. Substituting half of the carbon fiber volume with glass fibers will make

Correspondence to: Z. A. Mohd Ishak (zarifin@eng.usm.my).
Contract grant sponsor: Ministry of Science, Technology, and Environment, Malaysia; Contract grant number: IRPA 6010615.

the composites much cheaper. Other than that, carbon fibers and glass fibers have different engineering property levels toward different tests, e.g., thermal, flexural.[11] By using both glass and carbon fibers, we hope to make a composite that has unique property combinations that are not possible using a single fiber composite.

The coinjection molding process also brings about esthetic values in the samples, enabling the composites to be used for decorative purposes.[10] This is especially obvious when the skin is a transparent or opaque layer and the core is a darker layer (i.e., carbon fibers in the core and glass fibers in the skin layer).

The objective of this paper is to investigate the mechanical and fracture behavior of (co)injection molded PA 6 composites with short glass fiber (SGF)/short carbon fiber (SCF) hybrid reinforcement and to further characterize the failure mechanisms with particular interest in the sandwich structure composites produced using (co)injection molding. It is also our objective to further correlate the test results with the microstructural characterization results, to explain the trends observed, and to see the unique effects brought about by the (co) injection molded formulations.

EXPERIMENTAL

Materials

Short fiber composites of PA 6 glass fiber, carbon fiber, the hybrid blend, and two types of sandwich skin–core hybrids were used. The sandwich composites were compounded with a twin screw extruder (Labotex-300, produced by Japan Steel Works Co., Ltd.) and fabricated with a conventional injection molding machine and an 80-ton coinjection molding machine (FN1000, manufactured by Nissei Plastic Industrial Co., Ltd.). The coinjection molding machine is equipped with 80-ton clamping units and two injection units (A and B) with two 38-cm^3 injection units oriented at an angle of 25° to each other to shorten the sprue distance. The nozzle section of this machine is schematically shown in Figure 1a. The actions of the two injection units are independently controllable. This allows the adjustment of the time lag between the onsets of the two injections. Dumbbell-shape and square plaque molds were injected in the sequential mode. The material that would form the skin part was injected 1 s prior to the second material that would later form the core of the part. The injection time lag is set so that the core material reaches the gate at the time of the completion of the injection of skin material. The holding pressure was applied only by the injection unit of the core material after the completion of the cavity fill. The cavity design used for all composite formulations is shown in Figure 1b. In this design, the two runners with 6.00-mm circular cross sections pass the melt from the sprue to the gate. A rectangular gate (edge gate) is located at the nonmoving part of the rectangular plaque and dumbbell mold. The molding conditions for coinjection molding and conventional injection molding are presented in Tables I and II, respectively. All samples were produced with 200°C melt temperature and 40 s holding time. The densities for glass fibers, carbon fibers, and PA 6 are 2.60, 1.75, and 1.14 g/cm^3, respectively. The fiber volume fraction for all formulations was fixed at 0.07. A processing flow chart of the five formulations used in the experimental is presented in Figure 2.

The formulations were categorized as shown in Table I.

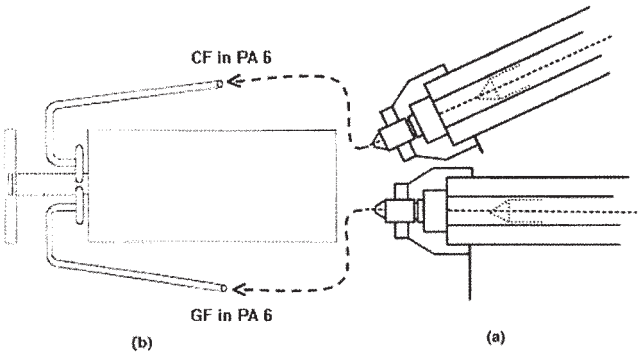

Figure 1 (a) Coinjection molding nozzle section. (b) Mold cavity.

TABLE I
Typical Formulations and Their Description

Formulations	Description
CF/PA 6	Short CF in PA 6
GF/PA 6	Short GF in PA 6
GF/CF/PA 6 hybrid	Short CF and GF in PA 6
CF_s/GF_c/PA 6	Short CF in skin and short GF in core
GF_s/CF_c/PA 6	Short GF in skin and short CF in core

Conditioning of specimens

All samples were conditioned at 80°C in a vacuum oven for a period of 72 h, in accordance to previous

TABLE II
Injection Molding Conditions for Co-Injection Molding

Co-injection molding parameters	Barrel A	Barrel B
Barrel temperature range (°C)	175–200	175–200
Maximum injection pressure (MPa)	10	7.5
Maximum screw speed (rpm)	160	175
Shot size (mm)	A1 = 30–55	
	A2 = 5	12–37
Nozzle temperature (°C)	200	200
Packing pressure range (MPa)	1–6	1–6

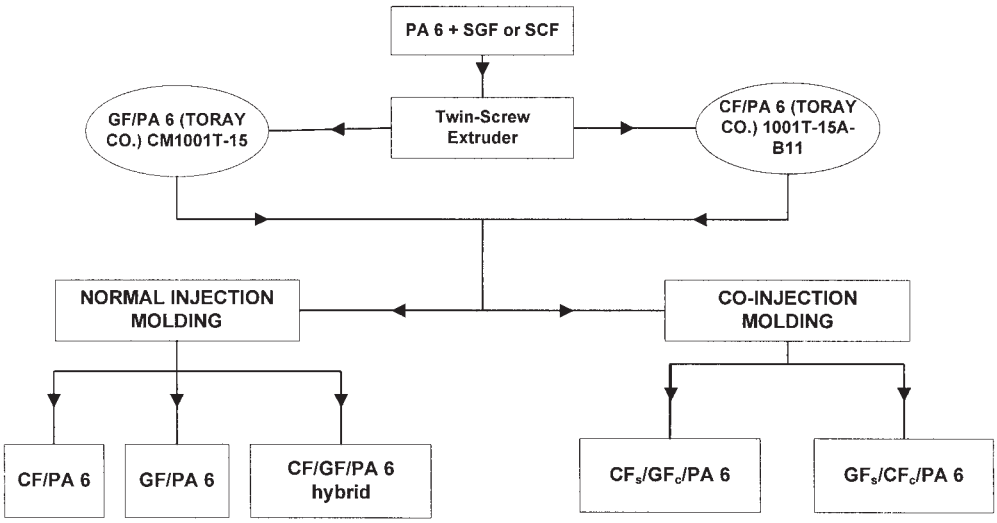

Figure 2 Flow chart of sample processing.

work done on similar materials.[12] This was done to remove most of the moisture that might have been absorbed due to the hygroscopic nature of the PA 6 matrix.

Testing and characterization

Microstructural characterizations

The DSC thermograms of slices cut from various depths of the samples (skin and core regions) were recorded by a Perkin–Elmer Model DSC-2. Samples weighing 10.00 mg were used. The samples were scanned from 30 to 300°C at a heating rate of 20°C/min. Analysis was performed under a nitrogen purge at a flow rate of 10 mL/min to prevent oxidative degradation. The degree of crystallinity, X_c, was calculated assuming a heat of fusion of the perfectly crystalline PA 6 samples to be the same as that of the pure polyamide 6,6 crystal, which is 130 J/g.[37]

The fiber alignment in different layers across the thickness of the composites was visualized wth the help of metallographically polished specimens and high contrast imaging in an Olympus PME3 microscope that was connected to a computer via a QB color CCD TV camera. The images obtained were recorded digitally in JPEG format.

Prior to imaging, the fracture surfaces of the single-edge notch-bending (SEN-B) test samples were polished using a double polishing machine, using abrasive sandpapers. The samples were then placed in rubber molds, embedded in epoxy resin, and left to dry. The embedded samples in epoxy were then polished again using sandpapers and finally with alumina powder. The determination of fiber length distribution followed after burning off the matrix in a vacuum furnace at 600°C in air and nitrogen atmospheres. Fibers obtained were dispersed in glycerol and observed under an Olympus PME3 optical reflectance microscope that was connected to a computer via a QB color CCD TV. The IMAPS analysis program was used to manually calculate the fiber lengths for each formulation. A minimum of 500 fibers was calculated for each formulation.

TABLE III
Injection Molding Conditions for Conventional Injection Molding

Injection molding parameters	
Barrel temperature range (°C)	175–200
Maximum injection pressure (MPa)	10
Maximum screw speed (rpm)	175
Shot size (mm)	55–92
Nozzle temperature (°C)	200
Packing pressure range (MPa)	1–6

Mechanical tests

The tensile test was done in accordance with ASTM Standard D638 on a Testometric tensile testing machine, using a crosshead speed of 1.00 mm/min.

The flexural test (three-point mode) was done in accordance with ASTM D 790–98. The specimen dimensions were 100.00 × 13.00 × 3.00 mm. The crosshead speed selected was 1.00 mm/min with a support span (L) of 64 mm. The specimens were cut parallel and transverse to the mold filling direction (MFD) and were labeled LT and TL, respectively (see Fig. 3a).

Fracture toughness

The fracture toughness, K_c, was determined according to ISO 13,586: 2000 using SEN-B specimens. The ap-

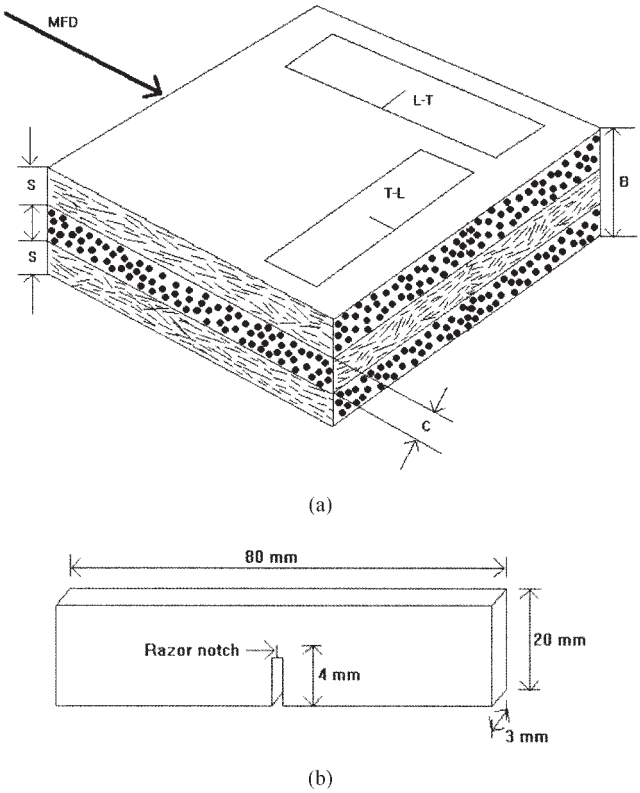

Figure 3 (a) Machining of the SEN-B test specimens used. (b) Designation of the SEN-B test specimens used.

plication of Linear Elastic Fracture Mechanics theory facilitates the evaluation of K_c values. The machining and designation of the SEN-B test samples are given in Figure 3a and b, respectively.

The SEN-B test specimens was machined from the injection molded plaques. Specimens with an initial notch cut transverse to the MFD were designated LT specimens, whereas specimens with notches cut longitudinal to the MFD were designated TL specimens according to the ASTM E616−81 standard. A natural crack was generated by tapping on a new razor blade placed in the notch. The SEN-B specimens were tested at a crosshead speed of 1.00 mm/min. The test was conducted at 20°C in ambient humidity. The values for K_c were calculated using the equation

$$K_c = \frac{P_c \frac{S}{4}}{B\frac{W^2}{6}}\left[1.93 - 3.07\left(\frac{a}{W}\right) + 14.53\left(\frac{a}{W}\right)^2 - 25.1\left(\frac{a}{W}\right)^3 + 25.8\left(\frac{a}{W}\right)^4\right], \quad (1)$$

where P_c = load at peak, N; B = specimen thickness, in meters; W = specimen width, in meters; a = notch length, in meters; S = span length, in meters.

The fracture energy, G_c, was calculated using the equation

$$G_c = \frac{K_c^2}{E}, \quad (2)$$

where K_c is the fracture toughness value and E is the elastic modulus value.

Scanning electron microscopy

The fracture surfaces were examined using a Cambridge scanning electron microscope (SEM) Model Leica *S*-360. SEM micrographs were taken at 25 kV high-acceleration voltage at various magnifications. Prior to the SEM observations, the fractured parts of the specimens were mounted on aluminum stubs and were sputter coated with a thin layer of gold to avoid electrical charging during examination.

RESULTS AND DISCUSSION

Microstructural characterization

Figure 4 illustrates DSC scans from both the skin and the core regions of the CF/GF/PA 6 blend formulation. A characteristic feature of all thermograms is recrystallization exotherms, which takes place during the heating process of the sample just before the main melting peak at T = 221°C. This phenomenon can be explained in terms of fast cooling at the mold wall during the injection molding process. The intensity of this peak diminishes if sliced DSC samples are taken from the core region, as there is no contact of core regions with the wall.[38] However, the peak does not diminish much in the core region of the composites, indicating an inner stress state of the matrix due to the presence of fibers. The enthalpy of crystallization, ΔH_c, established in cooling regimes for the matrix and the composites agreed with each other quite well. From the information obtained, the degree of crystallinity, χ_c, of all formulations could be calculated using the equation

$$\chi_c = \frac{\Delta H_c}{\Delta H_{m(\text{fullycrystallinePA6,6})}} \times 100\%, \quad (3)$$

where ΔH_c is the enthalpy of crystallization derived from the DSC scans, and $\Delta H_{m(\text{fully crystalline PA 6,6})}$ is the heat of fusion (130 J/g) of the 100% crystalline PA 6,6.[37]

Table IV shows the melt temperatures (T_m) and degree of crystallinity of the skin and core materials. Most T_m obtained from the DSC thermograms are very close to the actual T_m supplied by the matrix suppliers (220°C). The crystallinity of unfilled PA 6 is around 31–34%, as reported by other researchers.[32]

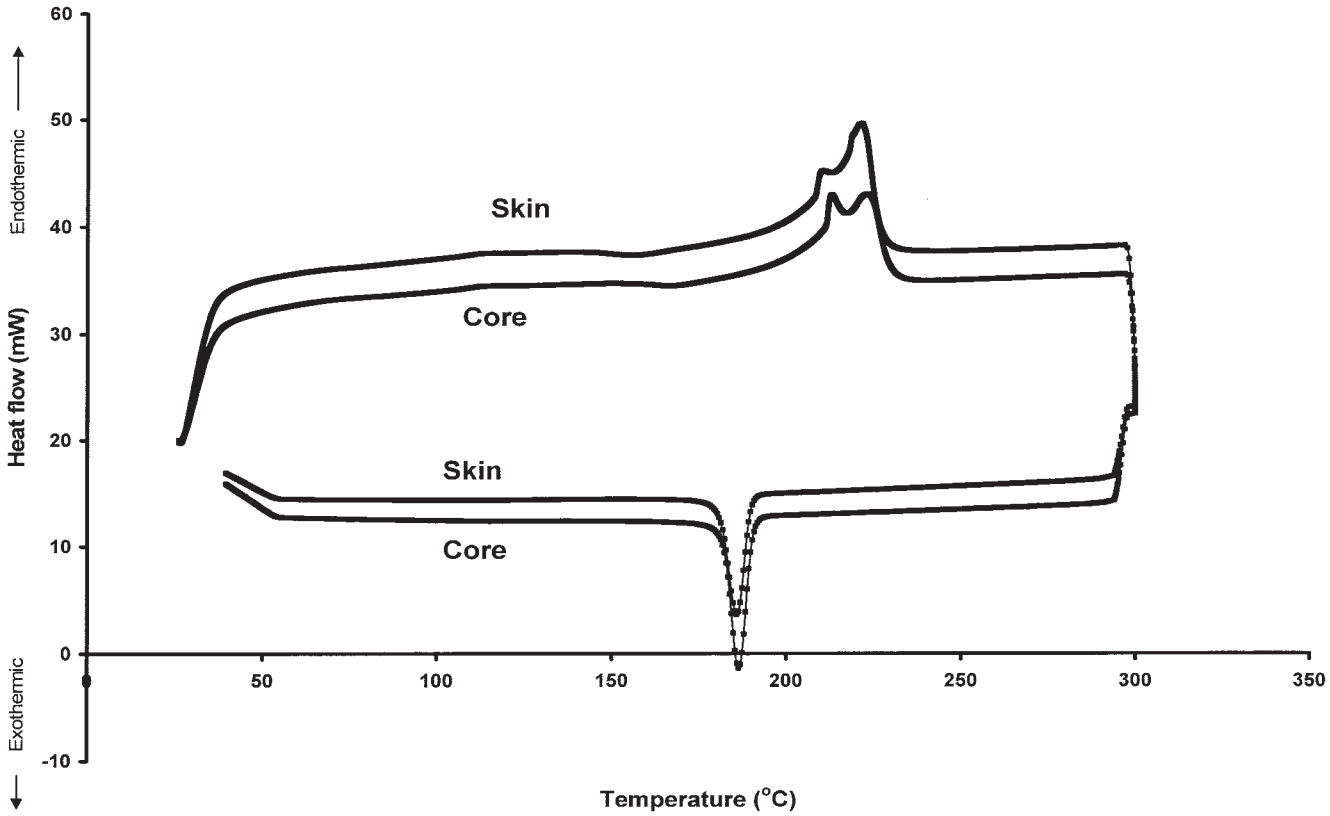

Figure 4 Characteristic DSC scans of the CF/GF/PA 6 blend formulation with skin and core results.

The reinforced PA 6 samples are observed to have slightly higher degrees of crystallinity. This indicates that some modification in the morphology of the PA 6 matrix has taken place as a result of the incorporation of fibers. The inner stress state explained earlier would account for this phenomenon. This recrystallization (sometimes referred to as cold crystallization or crystallization from the rubbery state[32]) is characteristic for semicrystalline thermoplastics with high melting temperatures processed by cold mold wall technology, as recently shown on the example of polyphenylene-sulfide.[33] A similar observation was made by Friedrich and Karger-Kocsis,[8] who have discovered that the intensity of the exothermic peak diminishes when the DSC samples were taken from the core region of the molded PA 6, 6. A very important point worth noting is that the regions containing carbon fibers in the CF_s/GF_c/PA 6 and GF_s/CF_c/PA 6 formulations show a very high degree of crystallinity compared to the regions containing glass fibers (either skin or core regions). This phenomenon further accentuates the fact that CF causes transcrystallinity in the PA 6 matrix, which will be explained in later parts of this paper.

Table IV also shows the composite densities, volume fraction, and the composite layering structure for each composite formulation. The fiber volume fraction values are maintained at a constant 0.07, as stated earlier. The skin layer is much thicker than the core layer. This is a result of strong elongational flows, resulting in a high

TABLE IV
Characterization of the PA 6 Composite Samples Used

Formulations	Density, ρ_c (g cm^{-3})	Layer structure		Melting temperature, T_m (°C)		Crystallinity (%)	
		2S/B	C/B	Skin	Core	Skin	Core
CF/PA 6	1.2	0.6	0.4	222.3	216.1	41.0	46.5
GF/PA 6	1.2	0.7	0.3	221.5	224.2	55.3	34.1
CF/GF/PA 6 hybrid	1.2	0.6	0.4	220.6	221.9	49.7	49.3
CF_s/GF_c/PA 6	1.2	0.6	0.4	221.9	223.2	53.5	38.1
CF_s/CF_c/PA 6	1.2	0.6	0.4	222.6	215.5	30.2	41.1

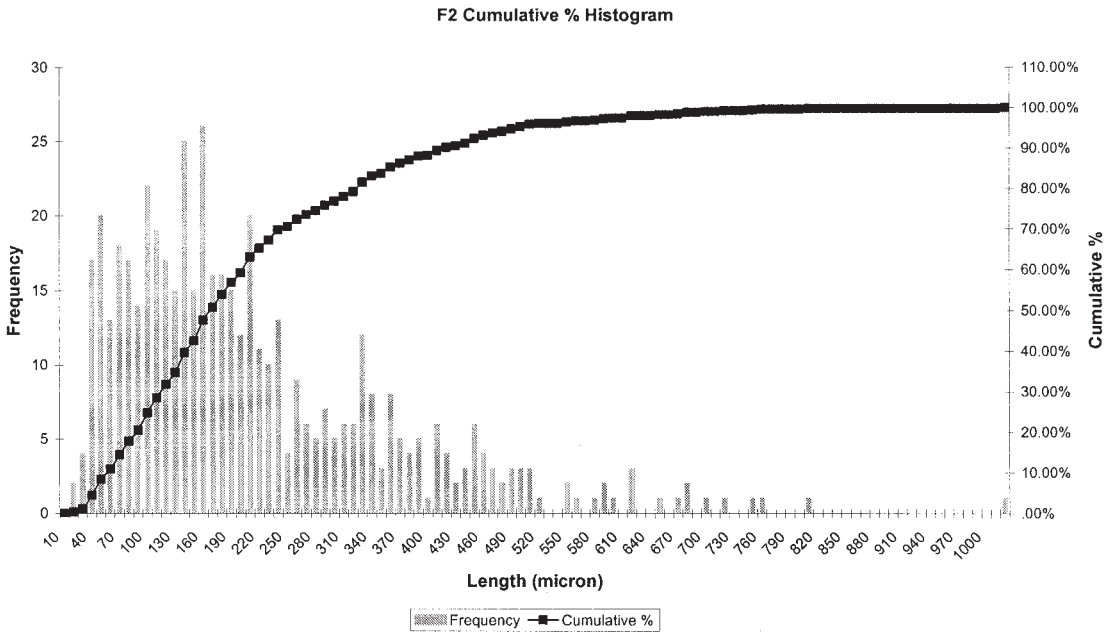

Figure 5 GF/PA 6 cumulative % histogram for fiber length (in micrometers).

fiber orientation parallel to MFD in the skin region. This happens as a result of there being less shear during the flow of the skin material into the mold.

A typical cumulative fiber length distribution curve for the glass fiber/PA 6 (GF/PA 6) formulation is given in Figure 5. The mean fiber lengths for various formulations are given in Table V. The mean fiber lengths have been seriously degraded compared to their initial lengths (~4 mm). The range of values obtained here are in agreement with other reported data of SFRTP composites.[18] The mean fiber lengths of glass fibers are clearly higher than that of the carbon fibers, be it in the individual composites with single types of fibers (GF/PA 6) or in the hybrid composites (CF/GF/PA 6 blend, CF_s/GF_c/PA 6 and GF_s/CF_c/PA 6) formulations. It is obvious that the retention of fiber lengths in the GF is better compared to CF in both conventional and hybrid composites, due to CF being more brittle compared to GF. As mentioned earlier, the phenomenon of fiber breakage is caused by many factors including fiber interaction with the viscous polymer melt during processing, the effect of processing equipments (extruder and injection molding machine) as well as fiber–fiber contact.

Tensile properties

Table VI shows the tensile properties of the various formulations. Both tensile strength and tensile modulus show a similar trend whereby the highest and lowest values are for CF/PA 6 and GF/PA 6 composites, respectively. These trends are expected due to the higher strength and stiffness of carbon fibers compared to glass fibers. The tensile strength and tensile modulus of the hybrid composites fall between these two single fiber systems. While carbon fiber/glass fiber/PA 6 (CF/GF/PA 6) blends and carbon fiber skin/glass fiber core/PA 6 (CF_s/GF_c/PA 6) have nearly the same values of strength and tensile modulus, glass fiber skin/carbon fiber core/PA 6 (GF_s/CF_c/PA 6) displayed slightly lower values. This indicates that the combination of CF/GF and CF_s/GF_c reinforces the PA 6 matrix much better compared to

TABLE V
Mean Fiber Lengths for Each Formulation (μm)

Formulation	Mean fiber length (μm)	
	Carbon fiber	Glass fiber
CF/PA 6	140	—
GF/PA 6	—	170
CF/GF/PA 6 hybrid	115	200
CF_s/GF_c/PA 6	117	197
GF_s/CF_c/PA 6	147	202

TABLE VI
Tensile Properties for Each Composite Formulation

Formulations	Tensile strength (MPa)	E-Modulus (GPa)	Elongation at break (%)
CF/PA 6	124.3	11.4	3.3
GF/PA 6	97.8	6.8	2.2
CF/GF/PA 6 hybrid	116.5	9.2	2.7
CF_s/GF_c/PA 6	112.1	9.3	3.1
GF_s/CF_c/PA 6	99.0	7.7	2.2

GF_s/CF_c, albeit the efficiency of reinforcement is not as good as the single CF system. Table VI shows that CF/PA 6 demonstrates the highest tensile properties. This may be attributed to the better nucleating ability of carbon fibers compared to glass fibers.[16] Several studies[2–4,34–36] have indicated that carbon fibers are capable of modifying the microstructure of the surrounding matrices by providing nucleating sites for crystalline growth.

The finer the fiber, the greater the probability of strength improvement, meaning that the probability of defect appearance is less. This is because, as the fibers get finer, its area per unit volume increases, providing more area for adhesion with the matrix. As such, carbon fibers being smaller in diameter provide better strength compared to glass fibers, which have larger diameters and thus smaller area per unit volume.

The results obtained also enable us to speculate that the hybrid effect (different types of fibers complimenting each other in terms of providing certain mechanical properties to the composite as a whole) becomes more significant as total volume fraction of reinforcement increases, as observed by others.[15] Packing defects may occur at higher fiber loading, which may reduce effective stress transfer from the matrix to the fibers. Uniformity in fiber dispersion decreases at higher loading. However, rapid crack propagation is hindered by the interlining fibers. The positive hybrid effect (described earlier) becomes more obvious as the mean fiber length decreases because there will be more fibers packed into a composite. The various orientations of the fibers in the matrix will further enhance the composites strength. However, care should be taken so that the fiber length is not below the critical fiber length needed to support loads effectively. Thus, the length of fibers used determines the degree of reinforcement in the composites. This is a very typical characteristic of the carbon and glass fiber reinforced composites.[6] The increase in tensile properties also hints that there is very good adhesion between the rough SCF surfaces and PA 6. This will be supported by SEM studies later in this paper. The tensile strength of the CF/GF/PA 6 blend hybrid is closer to that of CF/PA 6, indicating an advantage by substituting half of the SCF with SGF.

Table VI also shows the elongation at break (EB) values for the various conventional and hybrid composites. In all cases, the incorporation of either single fibers i.e., SGF or SCF, or hybrid fibers resulted in a dramatic reduction on the EB of PA 6. This is expected, as reported by other researchers.[12,17] This phenomenon occurs due to the reduction in free movement of the matrix when fibers are incorporated. The PA 6 matrix, which usually flows in a ductile manner (without reinforcement), finds that its flow is hindered by the incorporation of fibers. The hindrance in flow is both physical (matrix shrinking unto the fibers) and chemical (fibers reacting with the matrix to form bonds at the interface) in nature. These hindrances make the composites more brittle, resulting in lower EB values.

TABLE VII
Flexural Properties for Each Composite Formulation

Formulations	Flexural strength (MPa)		Flexural modulus (GPa)	
	L-T	T-L	L-T	T-L
CF/PA 6	177.6	117.0	7.9	3.5
GF/PA 6	163.8	106.0	4.7	2.8
CF/GF/PA 6 hybrid	175.4	128.1	6.0	3.5
CF_s/GF_c/PA 6	158.4	104.8	5.8	2.8
GF_s/CF_c/PA 6	125.8	98.4	4.4	2.6

Flexural properties

Table VII shows the flexural properties of the various composite formulations. The flexural data show the same trend as that obtained from tensile tests, i.e., CF/PA 6 having the highest strength and modulus. Synergism (positive hybrid effects) in the properties of GF/CF/polymer hybrid composites has been reported,[16,17] where both GF and CF in the same matrix complement each other. The effect is that the composites exhibit better properties not found in either CF/PA 6 or GF/PA 6 composites. This can be seen by referring to the CF/GF/PA 6 blend formulation, which exhibits better properties than the GF/PA 6 composites. The GF_s/CF_c/PA 6 sandwich composite actually shows lower flexural properties than CF_s/GF_c/PA 6. It is known that when stress is applied to the flexural sample, the core fails first, followed by the skin layer.[7] Carbon fiber, being more brittle than glass fiber, fails easily under applied stress. This immediately brings about a catastrophic failure in the skin layer and the whole sample. However, both sandwich composites show better properties than GF/PA 6 but poorer ones than CF/PA 6 and the hybrid CF/GF/PA 6 blend. This phenomenon could be because of the area per unit volume issue pertaining to glass and carbon fibers, as explained earlier. The higher surface roughness and better nucleating (transcrystallinity) abilities of carbon fibers compared to glass fibers would also bring about better properties in composites reinforced wholly or partially with carbon fibers. Flexural strength is a combination of the tensile or compressive strengths, which directly vary with the shear forces acting at the interface.[19] In flexural testing, various mechanisms such as tension, compression, and shearing will take place simultaneously and failures are said to occur as a combination of all these mechanisms.[26]

The damage of the composites in the L-T direction is dominated by fiber pull-out in tandem with matrix tearing and matrix microcracks caused by the fiber-ends and the breakage of fiber. On the other end, damage for the T-L samples are more toward fiber-matrix debonding and tearing of the matrix.[4]

Kretsis and Matthews,[21] in reviewing the flexural properties of the hybrid fiber reinforced plastics, reported that the flexural properties not only depend on the hybrid composition but also on the arrangement of the material layers. Skin–core morphologies are common among injection molded specimens, with the fibers lying longitudinally in the skin layers, implying higher load-bearing capabilities, and transversely in the core layer. L-T specimens and T-L specimens, as such, would also have different orientations for their skin and core, with the L-T specimens having two layers of longitudinally aligned fibers and the T-L specimens having a single layer of longitudinally aligned fibers. This results in lower flexural properties for the T-L specimens compared to the LT specimens. The fiber orientation of T-L and L-T specimens are depicted in Figure 3a for better understanding.

Fracture toughness and fracture energy

The values of K_c for the SEN-B test are shown in Table VIII. It is obvious in the skin–core hybrid composites that the K_c values are naturally higher for the L-T specimens compared to the T-L specimens. This, as explained earlier, is attributed to the skin and core structure. The L-T specimens have two layers of fibers lying longitudinally, providing more resistance through fiber pull-out in the composites. On the other hand, the T-L specimens have two layers of fibers lying transversely, providing less resistance toward fracture as fiber debonding occurs when the fibers are transversely aligned, contrary to fiber pull-out when the fibers are longitudinally aligned. Obviously, the fiber pull-out demands more energy compared to fiber-matrix debonding.

CF/PA 6 shows the highest K_c values. This is followed by the fiber blends, the sandwich composites, and last, GF/PA 6 with the lowest values. Justifying the high mechanical tests values of CF/PA 6 in accordance to the volume per unit area of fibers, the carbon fibers have more interaction with the PA 6 matrix. There is more area for the PA 6 to adhere (shrink) on CF compared to GF, because CF has a higher aspect ratio compared to GF.[38] Thus, the energy absorbing mechanism that arises from the energy required to pull out the carbon fibers from the matrix and fracturing the matrix is much higher compared to that of the glass fiber composites.[39] In addition, carbon fibers have a rougher surface morphology compared to glass fibers, providing better adhesion and additional friction in the event of failure. In reviewing the microstructure and fracture mechanical performance of SFRTPs, Karger-Kocsis[17] has noted that both the matrix- and the fiber-related mechanisms are responsible for determining the course of the K_c versus V_f curves.

TABLE VIII
Fracture Toughness and Fracture Energy Results for All Composite Formulations

Formulations	Fracture toughness, K_c (MPa · m½)		Fracture energy, G_c (kJ/m^2)	
	LT	TL	LT	TL
CF/PA 6	8.6	5.4	9.3	8.5
GF/PA 6	5.7	4.0	6.9	5.6
CF/GF/PA 6 hybrid	8.1	5.1	11.0	7.4
CF_s/GF_c/PA 6	7.4	4.7	9.5	7.8
GF_s/CF_c/PA 6	7.2	4.8	11.6	8.9

A micrograph of the fractured SEN-B samples is presented in Figure 6. The L-T sample has a crack that swerves during testing, contrary to the T-L samples that have a straight fracture line. The fiber layering in the L-T specimens force the cracks to follow this zig-zag path associated with considerable energy dissipation, as well as fiber avoidance mechanisms, as explained by Szabo and Czigany[4] and other researchers.[16]

The K_c values in Table VIII also show that the CF_s/GF_c/PA 6 has higher fracture toughness compared to the GF_s/CF_c/PA 6 hybrid composites. Carbon fibers, being more brittle compared to glass fibers, are also known to increase the strength and fracture toughness of composites. Using a higher V_f of "strength contributing" component naturally would bring about better mechanical and fracture properties to the composites.

Graphs obtained from the fracture test (load-displacement) show a very smooth curve, indicating gradual yielding of the sample. The samples gradually yield under increased load and subsequently fail as the fracture spreads throughout the sample. This was concluded based on the well-discernible, smooth crack propagation range after the maximum load, F_{max}, was reached. This is explained in terms of fiber fracture. Once fibers fracture, the stress decreases accordingly. Thereby, crack bridging and fiber pull-out are the toughening mechanisms. The rough fracture surface of the composites show that crack deflection should be another toughening mechanism because the crack swerving and twisting along the fiber/matrix interface consumes more energy than cracks propagating directly.[28] The three toughening mechanisms, namely crack bridging, fiber pull-out, and crack deflections, operate simultaneously during crack propagation. It is very difficult to experimentally identify the relative contributions and the role of each toughening mechanism.[28]

Figure 6 GF/PA 6 SEN-B specimens, L-T and T-L orientations.

Table VIII also gives the critical strain energy release rate or fracture energy values, G_c, of each individual formulation in both LT and TL orientations. At any given formulation, it can be observed that the LT specimens give higher G_c values compared to the TL specimens. As explained earlier in the case of K_c, this arises as a result of different fiber orientation and layering in the two types of specimens. The GF_s/CF_c/PA 6 formulation has the highest G_c values, followed by the CF/GF/PA 6 blend. The GF/PA 6 formulation has the lowest values, a fact that could be attributed to the lower aspect ratio of the glass fibers compared to carbon fibers.[39] The CF/GF/PA 6 blend has reasonably high G_c values. From these results, it can be inferred that glass fiber in itself provides less resistance to fracture. However, if both glass and carbon fibers are combined, there is very good synergism between both fibers, which in turn can hinder fracture growth. However, the CF_s/GF_c/PA 6 has reasonably low fracture energy values. This is attributed to the adhesion efficiency of the GF core. GF, having weaker adhesion with the matrix due to its smooth surface, along with its inability to cause transcrystallinity, fails fast and brings about less energy to fracture the whole sample. There is also another inference that can be made concerning the CF/PA 6 formulation. It can safely be said that although carbon fibers are brittle compared to glass fibers, they tend to bring about better fracture resistance when used as the only form of reinforcement, in contrast to glass fibers that provide little fracture resistance. This phenomenon, again, is related to the aspect ratio and transcrystallinity ability of CF and GF. Other literatures further observe that the G_c values increase with increasing fiber volume fraction and lower temperatures.[16] Karger-Kocsis[17] has also observed that the G_c values increase with increasing fiber content. These observations give room for further research in the same area and will be considered in subsequent papers.

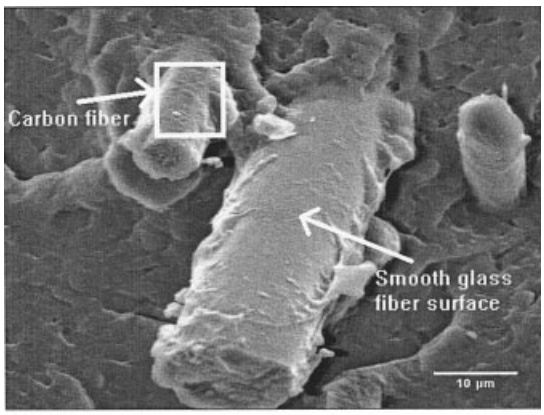

(a)

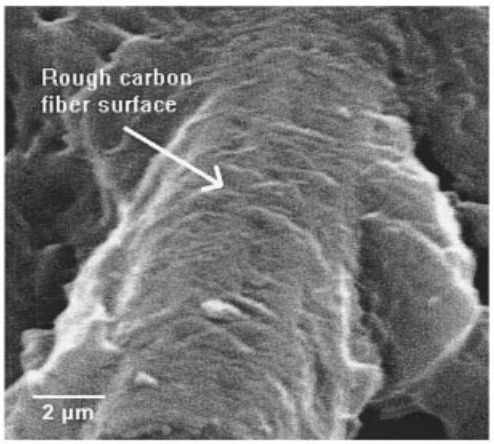

(b)

Figure 7 (a) SEM micrographs taken from the fracture surface of GF/CF/PA6 blend showing the appearance of CF and GF. (b) SEM micrographs taken from the fracture surface of GF/CF/PA6 blend showing an enlarged portion of the CF fiber.

Morphology

Figure 7a and b shows the surface appearance of glass and carbon fibers in GF/CF/PA6 blend. Good fiber–matrix interaction between PA 6 and carbon or glass fibers is seen in both Fig. 7a and b. The PA 6 matrix can be seen to adhere or wet the carbon and glass fibers in the GF/CF/PA 6 blend. It can also be observed that carbon fibers naturally have a rougher surface finish (cf. Fig. 7b) than glass fibers. As such, there should be a better adhesion of the matrix with the carbon fibers compared to the smooth glass fiber surfaces. This observation has also been made by Tjong et al.[29] as well as by Mohd Ishak and Berry.[30] There is also a great difference in the size of carbon fibers and glass fibers, taken at the same magnification, removing any doubt regarding which is which. Carbon fibers are smaller in diameter compared to glass fibers. Concluding remarks cannot be made regarding the nucleating ability of the carbon fibers from the SEM micrographs.

From Figure 8 it can be deduced that the most common failure that occurred is through fiber pull-out. This phenomenon can be observed in both glass and carbon fiber. Fiber pull-out is indicated by the holes (indicated by arrows in Fig. 8). Ductile matrix failure is also observed at the matrix.

Figure 9 shows the notch area of the CF/GF/PA 6 blend formulation from the SEN-B test. The razor notch formed as a result of tapping a blade on the notch, as explained in the experimental section. Fiber pull-out and debonding are evident near the notch.

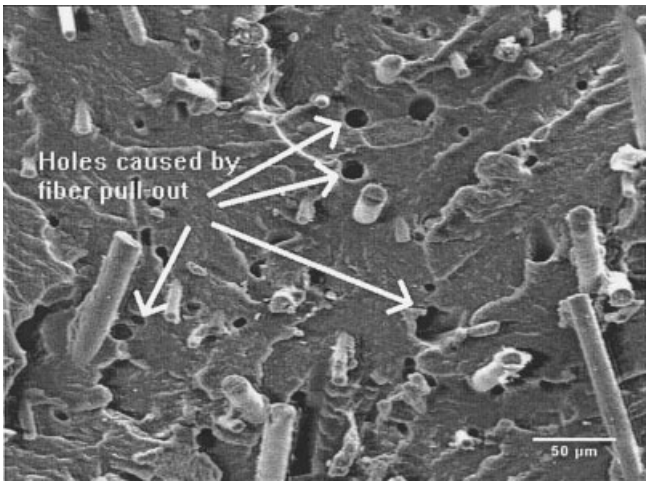

Figure 8 SEM micrographs showing the occurrence of fiber pull-outs in the PA 6 matrix.

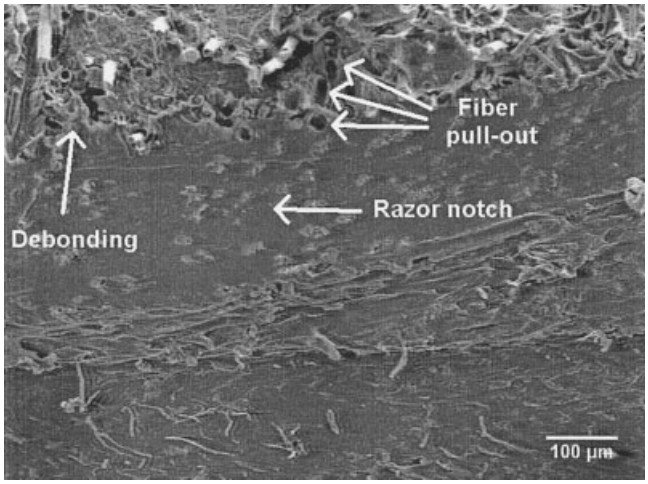

Figure 9 SEM micrograph of CF/GF/PA 6 blend composite showing matrix debonding and fiber pull-out.

CONCLUSIONS

This paper reports on the influence of both internal parameters (volume fraction of fibers, skin–core morphology, and degree of crystallinity) and external parameters (orientation of sample, i.e., LT and TL) on the mechanical and fracture behavior of (co)injection molded PA 6 composites with short glass fiber/short carbon fiber hybrid reinforcement. The conclusions from this study can be summarized as follows.

1. CF/PA 6 exhibits the highest values for each mechanical and fracture test due to the higher strength and stiffness of carbon fibers compared to glass fibers. There is better adhesion between carbon fibers and PA 6 compared to glass fibers due to surface roughness. DSC results confirmed that carbon fibers also have better nucleating abilities compared to glass fibers.

2. The skin–core sandwich composites exhibit only moderate values for each mechanical and fracture test However, the CF_s/GF_c/PA 6 composites exhibit higher mechanical properties compared to GF_s/CF_c/PA 6 composites. The hybrid composite blends give the most optimum mechanical and fracture properties, indicating the advantage of substituting half of the CF with GF, which would provide a more feasible material costs.

3. The composite damage in L-T specimens are due to fiber pull-out along with matrix tearing and matrix micro cracks caused by fiber breakages and fiber ends, giving it higher mechanical values compared to T-L specimens, which are primarily damaged due to debonding of fibers and matrix.

Kyoto Institute of Technology and Toray Japan are acknowledged for supplying the materials used in this study.

References

1. Kohan, M. I. Nylon Plastics Handbook; Hanser: New York, 1995; Chapter 10, p 258.
2. Folkes, M. J Short fiber reinforced plastics. In Multicomponent Polymer Systems; Miles, I. S.; Rostami, S., Eds.; Longman Scientific and Technical: Essex, 1992; Chapter 8, p 207.

3. Krenchel, H. Fiber Reinforcement; Akademisk Forlag: Copenhagen, 1964.
4. Szabo, J. S.; Czigany, T. Static fracture and failure behavior of aligned discontinuous mineral fiber reinforced polypropylene composites. Polym Test 2003, 22, 711.
5. Parratt, N. J. Fibre Reinforced Materials Technology; Van Nostrand Reinhold: London, 1972.
6. McCrum, N. G. A Review of the Science of Fiber Reinforced Plastics; HMSO: London, 1971.
7. Hitchen, S. A.; Kemp, R. M. J. Development of novel cost effective hybrid ply carbon-fiber composites. Compos Sci Technol 1996, 56, 1047.
8. Friedrich, K.; Karger-Kocsis, J. In Fractography and Failure Mechanisms of Polymers and Composites; Roulin-Moloney, A. C., Ed.; Elsevier Applied Science: London, 1989; p 437.
9. Li, R. K. Y.; Lu, S. N.; Choy, C. L. Tensile and compressive deformation of a short-glass-fiber-reinforced liquid crystalline polymer. J Thermoplast Comp Mater 1995, 8, 304.
10. McRoskey, J. Lower material costs? Fewer design constraints? Molding Syst 2000, 58, 28.
11. Moss, M. D.; Dynisco, Inc. Hot runners boost coinjection molding process. Modern Plast Int 1997, 27, 74.
12. Looi, C. M. Hygrothermal and Fracture of Injection Molded Short Glass Reinforced Polyamide 6; M.Sc. Thesis; Universiti Sains Malaysia, 2001.
13. Friedrich, K.; Karger-Kocsis, J. Fracture and fatigue of unfilled and reinforced polyamides and polyesters. In Solid State Behavior of Linear Polyesters and Polyamides; Schultz, J. M.; Fakirov, S., Eds.; Prentice Hall: Englewood Cliffs, NJ, 1990; p 249.
14. Fu, S.Y.; Xu, G.; Mai, Y. W. On the elastic modulus of hybrid particle/short fiber/polymer composites. Compos B 2002, 33, 291.
15. Fu, S. Y.; Lauke, B.; Mäder; E.; Hu, X.; Yue, C. Y. Fracture resistance of short-glass-fiber-reinforced and short-carbon-fiber-reinforced polypropylene under Charpy impact load and its dependence on processing. J Mater Process Technol 1999, 89–90, 501.
16. Mohd Ishak, Z. A.; Ishiaku, U. S.; Karger-Kocsis, J. Microstructure-related fracture behavior of injection molded short fiber reinforced polyarylamide in dry and wet states. J Mater Sci 1998, 33, 3377.
17. Karger-Kocsis, J. Microstructure and fracture mechanical performance of short-fiber reinforced thermoplastics. In Application of Fracture Mechanics to Composite Materials; Friedrich, K., Ed.; Elsevier: Amsterdam, 1989; p 189.
18. Ishiaku, U. S.; Hamada, H.; Mizoguchi, M.; Takashima, S.; Chow, W. S.; Mohd Ishak, Z. A. The effect of ambient moisture and temperature conditions on the mechanical properties of glass fiber/carbon fiber/PA 6 sandwich hybrid composites consisting of skin-core morphologies; ANTEC Proceedings 2003, Nashville, TN, 2003; p 2142.
19. Tjong, S. C.; Meng, Y. Z. Morphology and mechanical characteristics of compatibilized polyamide 6-liquid crystalline polymer composites. Polymer 1997, 38, 4609.
20. Shan, Y.; Liao, K. Environmental fatigue of unidirectional glass–carbon fiber reinforced hybrid composite. Compos B Eng 2002, 32, 355.
21. Kretsis, G.; Matthews, F. L. The strength of bolted joints in glass fiber/epoxy laminates. Composites 1985, 16, 92.
22. Peijs, A. A. J. M.; Catsman, P.; Govaert, L. E.; Lemstra, P. J. Hybrid composites based on polyethylene and carbon fibers Part 2: Influence of composition and adhesion level of polyethylene fibers on mechanical properties. Composites 1990, 21, 513.
23. Koenig, J. L. Chemical microstructure of polymer chains. J Mol Struct 1982, 78, 134.
24. Marom, G.; Tuler, F. R.; Wagner, H. D. Time and temperature dependence of fracture in a unidirectional glass-reinforced epoxy. Polymer 1979, 20, 653.
25. Zweben, C. Tensile strength of hybrid composites J Mater Sci 1977, 12, 1325.
26. Sreekala, M. S.; George, J.; Kumaran, M. G.; Thomas, S. The mechanical performance of hybrid phenol-formaldehyde-based composites reinforced with glass and oil palm fibers. Compos Sci Technol 2002, 62, 339.
27. Mandell, J. F. Fatigue behavior of short fiber composite materials. Fatigue of Composite Materials; Reifsnider, K. L., Ed.; Elsevier: Amsterdam, 1991; Chapter 7, p 231.
28. Song, G. M.; Li, Q.; Wen, G. W.; Zhou, Y. Mechanical properties of short carbon fiber-reinforced TiC composites produced by hot pressing. Mater Sci Eng A 2002, 326, 240.
29. Tjong, S. C.; Xu, S. A.; Li, R. K. Y.; Mai, Y. W. Short glass fiber-reinforced polyamide 6,6 composites toughened with maleated SEBS. Comp Sci Technol 2002, 62, 2017.
30. Mohd Ishak, Z. A.; Berry, J. P. Impact properties of short carbon fiber reinforced nylon 6, 6. Polym Eng& Sci 1993, 33, 1483.
31. Hahn, M. T.; Hertzberg, R. W.; Manson, J. A. Infrared measurement of specimen temperature profiles during fatigue crack propagation tests. Rev Sci Instrum 1983, 54, 604.
32. Cebe, P.; Hong, S. D. Crystallization behavior of poly (ether-ether-ketone). Polymer 1986, 27, 1183.
33. Karger-Kocsis, J.; Friedrich, K. Microstructural details and the effect of testing conditions on the fracture toughness of injection-molded poly (phenylene-sulphide) composites. J Mater Sci 1987, 22, 947.
34. Li, T. Q.; Zhang, M. Q.; Zeng, H. M. A preliminary proof on the quasi-epitaxial growth of a semicrystalline polymer in its short carbon fiber composites. J Mater Sci Lett 1999, 18, 1861.
35. Li, T. Q.; Zhang, M. Q.; Zhang, K.; Zeng, H. M. Long-range effects of carbon fiber on crystallization of semicrystalline thermoplastics. Polymer 2000, 41, 161.
36. Lovinger, A. L.; Hudson, S. D.; Davis, D. D. High-temperature crystallization and morphology of poly (arylether ether ketone). Macromolecules 1992, 25, 1752).
37. Karger-Kocsis, J.; Friedrich, K. Fracture behaviour of injection-molded short and long glass fiber polyamide 6,6 composites. Comp Sci Tech 1988, 32, 293.
38. Karger-Kocsis, J.; Harmia, T.; Czigany, T. Comparison of the fracture and failure behaviour of polypropylene composites reinforced by long glass fibers and by glass mats. Comp Sci Technol 1995, 54, 287.